J Mater Sci (2009) 44:2966–2976
DOI 10.1007/s10853-009-3393-z

Microstructure and texture assessment of Al–Mn–Fe–Si (3003) aluminum alloy produced by continuous and semicontinuous casting processes

J. P. Martins · A. L. M. Carvalho · A. F. Padilha

Received: 15 September 2008 / Accepted: 11 March 2009 / Published online: 7 April 2009

Abstract Aluminum sheets are currently produced by the direct-chill process (DC). The need for low-cost aluminum sheets is a challenge for the development of new materials produced by the twin roll caster (TRC) process. It is expected that sheets produced from these different casting procedures will differ in their microstructure. These differences in microstructure and in the crystallographic texture have great impact on sheet mechanical properties and formability. The present study investigated microstructure and evaluated texture of two strips of Al–Mn-Fe–Si (3003) aluminum alloy produced by TRC and by hot-rolling processes. It was possible to notice that the microstructure, morphology, and grain size of the TRC sample were more homogenous than those found in hot-rolled samples. Both strips, obtained by the two processes, showed strong texture gradient across the thickness.

Introduction

First studies concerning utilization of Al–Mn alloys have been cited in 1902. Such alloys have been used commercially since 1910. Among the Al–Mn system, also known as the 3XXX alloys series, the most widely used is the 3003 alloy [1]. Owing to their good conformability, corrosion resistance, weldability, and allied reasonable mechanical resistance, they are becoming very interesting materials. They are commonly used in the shape of plates and sheets, and can also be extruded or forged, although their use in this form has been limited. Some examples of final applications are food packing (e.g., cans and domestic utensils), tiles, and heat exchangers [1].

One great advantage of these alloys is attributed to their composition variation and the presence of solute in solid solution. Although their optimum composition has relatively narrow limits, small variations do not substantially affect their manufacture or properties. The alloy generally allows 0.5% Fe and tolerates small amounts of Zn, Mg, and Ni; therefore, it can be produced from secondary aluminum [1].

Moreover, from the equilibrium diagram for the 3003 alloy, it can be verified that it is characterized by main Al phase with Al_6Mn and $Al_{15}(FeMn)_3Si$ particles. Addition of Mg slightly reduces the melting point of aluminum alloy. Its limit of solid solubility is 1.8% at eutectic temperature. The Al_6Mn phase from the 3003 alloy is formed as primary phase containing 1.9–4.1% Mn. Solution with higher Mn content is formed by peritectic reaction between Al_6Mn and liquid phases at 710 °C [2].

Under normal solidification conditions there is formation of primary dendritic of Al, and alloying elements concentrate at the interdendritic space until Al_6Mn nucleation occurs. However, with slow cooling, nucleation of precipitates is delayed, and in this way the Al–Al_6Mn eutectic tends to grow in a competitive way. Accordingly, Al_6Mn crystals grows in needle shape. In the case of fast cooling a decrease of Al_6Mn precipitates size occurs and the solid solution is saturated with Mn [3, 4].

The technology of the twin roll caster process has been described by Berg et al. [5] and in detail by Strid [6] and Merchant et al. [7]. The twin roll caster process produces coilable strip directly from the melt by combining casting

J. P. Martins (✉) · A. F. Padilha
Departamento de Engenharia Metalúrgica e de Materiais, Escola Politécnica, USP, São Paulo 05508-900, Brazil
e-mail: jpaula@usp.br

A. L. M. Carvalho
Departamento de Engenharia de Materiais, Universidade Estadual de Ponta Grossa, Ponta Grossa, PR 84030-900, Brazil

and hot rolling into a single step [8–10]. In twin roll caster, molten metal is fed onto water-cooled rolls, where it solidifies, and is then rolled, producing sheet directly from the melt [11]. For strips of 6–7 mm thickness the cooling rate is around 100–1,000 °C/s and dendritic spacing varies between 5 and 10 μm. Currently the twin roll caster process can produce strips up to 2.5 mm thickness. The greatest advantage of the roll caster process is elimination of the hot-rolling process, that is, it is a shorter process route that combines casting and dynamic hot deformation down to a few millimeter gage sheet in a single step when compared with direct chill casting. Moreover, it has greater flexibility than conventional productive processes, being widely used in applications where there is a wide range of products and a specific market. However, the twin roll caster process is limited to casting for only some alloys, such as the 1XXX, 3XXX alloys series, and some of the 5XXX series [12–14].

On the other hand, the greatest barrier to wider use of aluminum plates, mainly in the automobile industry, is high cost compared with steel. However, production of aluminum plates by twin roll caster process instead of conventional direct chill casting and the consequent elimination of hot rolling offers the opportunity to reduce the cost of aluminum plates substantially.

Broadly speaking, alloys obtained from the twin roll caster process exhibit high concentration of alloying elements in solid solution, fine intermetallic primary particles, and small grain size [15]. All these phenomena affect alloy behavior during thermomechanical processing. This is attributed to the high solidification rate observed in the twin roll caster process, which produces microstructure significantly different from that observed in the direct chill process followed by hot rolling. These microstructural differences as exhibited in the crystallographic texture have a strong influence on the mechanical properties and formability of aluminum alloy sheets. Therefore, the twin roll caster process has been increasingly applied in the aluminum rolling industry. The main aim of the present work is to show the microstructure and texture evaluation, through the thickness of the strip, of 3003 aluminum alloy obtained from the twin roll caster process (continuous ingoting) and the direct chill process (semicontinuous) followed by homogenization and hot rolling.

Experimental procedures

Materials

Commercial aluminum alloy 3003 was analyzed and its chemical composition was determined by atomic absorption spectrometer (ARL, model 3460). Two strips from the same alloy were compared in this work: one produced by twin roll caster process (as-cast) and another produced by direct chill process (DC, followed by homogenization and hot rolling). The alloy produced by twin roll caster process was supplied by Companhia Brasileira de Alumínio (CBA) in strips of 7.4 mm thickness. Currently, CBA produces, on average, 3 coils/day. The twin roll caster have been produced coils with two differents width, the narrow one has 9 ton and the wide one has 14 ton. Concerning the twin roll caster speed, the range has been 700–1,000 mm/min. The alloy produced by hot rolling had 6 mm thickness. Both strips were grinder-machined for analysis through their thickness.

Microstructural evaluation

Microstructures and textures (macrotexture and microtexture) were analyzed through strip thickness. Namely, evaluations were carried out at three positions: at the surface, at the center (halfway through), and at one-quarter thickness. This microstructural characterization was performed by: (a) light microscopy with polarized light and dark field, (b) scanning electron microscopy (SEM), and (c) transmission electron microscopy (TEM). Grain structure was examined under polarized light on samples anodically oxidized in Barker's reagent. Particles were observed after etching in 0.5% HF water solution. Samples for analysis by TEM were electrolytic polished in solution contains $HClO_4$. Electric conductivity was measured by a contact digital instrument (DC-09 model). Precipitates were evaluated by extraction technique using $HClO_4$ as electrolyte. After extraction, precipitates were washed and then analyzed in a Philips MPD 1880 model X-ray diffractometer, with CuK_α radiation. Other precipitates extraction methods have been investigated and compared [16].

Texture analysis

Texture analysis was carried out by the X-ray back-reflection goniometric method. Rigaku DMAX-2000 diffractometer was used for texture analysis, with CuK_α radiation. Pole figures (PFs) 111, 220, 200, and 311 were measured and then the orientation distribution functions (ODF) were obtained. Texture evaluation by electron backscattering diffraction (EBSD) with SEM was also carried out. The SEM was equipped with TSL hardware and software system. Electrolytic polishing was used in order to prepare samples with deformation-free surface suitable for EBSD analysis.

Results and discussion

Microstructure

In the twin roll caster process, the metal enters the rolling zone at temperature close to the alloy melting point. Metal

solidification starts at the first point of contact with the rolls, that is, before the roller bite point. The processing volume may be divided into three regions as follow: (a) liquid zone, (b) mushy zone, and (c) hot-rolling (or reduction) area. In the liquid zone, the metal loses heat to the atmosphere and crystal solidification starts. In the mushy zone, crystals are formed and immediately grow. In the last zone, in which the metal is solidified, the metal undergoes deformation due to the rollers, and metal grains grow in the rolling direction. In this phase, plastic deformation of the metal between the rollers occurs, and it leaves the rollers at a temperature close to 300 °C. The deformation, therefore, occurs in a temperature range between the solidus line and 300 °C [17]. The exit temperature of the metal is relatively low in order to avoid recrystallization, and as a consequence the strip is deformed. In a similar study, it was verified that deformation introduced during the twin roll caster process corresponded to a range of 10–25% reduction in area compared with cold rolling [18].

Table 1 shows the chemical composition of strips produced by hot-rolling and by twin roll caster processes in three different positions: surface, one-quarter thickness, and in the center of strip thickness. One can note that there is no difference in chemical composition through the thickness.

Vickers microhardness values from hot-rolled and twin roll caster strips in the three different positions are presented in Table 2, showing that there was a small difference through the thickness, with larger deformation at the surface. These values were as expected, owing to the higher pressure required on the surface of the strip from the rollers. However, this difference in microhardness values through the thickness has no relation with alloy composition, as shown by Table 1, as there is no significant variation in chemical composition with thickness.

This suggests that the difference in microhardness between the twin roll caster and hot-rolled samples can be explained by the hardening mechanisms. The five most common hardening mechanisms are: (a) deformation (strain hardening), (b) grain-refine hardening, (c) solid-solution hardening, (d) coherent precipitation hardening, and (e) dispersion incoherent particles hardening. Basically, plastic deformation hardening is an effective mechanism; however, it is limited by deformation temperature and to metals that display a higher hardening coefficient, e.g., those with low stacking fault energy. The deformation hardening occurs due to arresting dislocation. Grain-refine hardening follows the Hall–Petch equation ($\sigma = \sigma_0 + k(d)^{-1/2}$, where σ_0 is the initial yield stress, k is a constant, and d is grain diameter), which also relates the yield stress to grain size; therefore, it is not very effective due to the difficulty in obtaining material with sufficient grain size to result in efficient hardening. Besides, grain-refine hardening is caused by grain boundaries, which are barriers to the motion of dislocations. Solid-solution hardening is an important mechanism, but is limited in the case of aluminum owing to the low solubility of the most common solute, i.e., solute atoms in the solid solution distort the crystalline lattice matrix (with the solid solution interstitial being more effective), thus impeding the motion of dislocations. Although coherent precipitation hardening produces alloys with high resistance, in this case the precipitate does not arrest all dislocation motions: when the precipitates are sheared an antiphase boundary appears and the interface surface increases. Dispersion incoherent particles hardening enhances the number of dislocations (through the formation of dislocation rings). The 3003 alloy in this study does not present coherent precipitates; that is, it is not hardenable by thermal treatment. Therefore,

Table 2 Vickers microhardness values from the hot-rolled and twin roll caster strips through their thickness: at the surface, one-quarter thickness, and in the center of strip

Process: position	Microhardness (HV) (300 g)
Rolled strip: surface	41.54 ± 0.61
Rolled strip: ¼	40.08 ± 0.60
Rolled strip: center	41.23 ± 0.70
Twin roll caster strip: surface	53.95 ± 0.7
Twin roll caster strip: 1/4	51.70 ± 1.23
Twin roll caster strip: center	52.02 ± 1.3

Table 1 Chemical composition (wt%) from the hot-rolled strip and the twin roll caster strip in the three positions: on the surface, one-quarter thickness, and in the center of strip

Process: position	Si	Fe	Mg	Mn	Cu	Cr	Ni	Ti	V	Zn	Ga	B
Rolled strip: surface	0.197	0.575	0.02	0.998	0.132	0.007	0.003	0.015	0.006	0.011	0.012	0.001
Rolled strip: 1/4	0.198	0.577	0.02	1.004	0.132	0.007	0.003	0.015	0.006	0.011	0.012	0.001
Rolled strip: center	0.2	0.581	0.02	1.002	0.133	0.007	0.003	0.016	0.006	0.011	0.012	0.002
Twin roll caster strip: surface	0.084	0.631	0.001	1.224	0.236	0.004	0.002	0.024	0.008	0.009	0.012	0.003
Twin roll caster strip: 1/4	0.083	0.630	0.001	1.223	0.236	0.004	0.003	0.029	0.008	0.009	0.013	0.004
Twin roll caster strip: center	0.084	0.631	0.001	1.221	0.236	0.004	0.002	0.028	0.008	0.009	0.013	0.004

the difference in microhardness values (Table 1) observed between the two samples from the twin roll caster and hot-rolling processes may be explained based on the deformation or strain-hardening hardening mechanism. Comparing Figs. 1a, b and 2a, b, one can see that the dislocation density for the twin roll sample is higher that that for the hot-rolled sample. This suggests that the twin roll caster sample suffered considerable plastic deformation during its processing; cell structure and dislocations in subgrains can be observed (Fig. 1a, b). Moreover, the difference in microhardness may be associated with lower grain size for the twin roll caster sample (Fig. 3a, b). Moreover, this can be attributed to the amount of solute in the solid solution, owing to the high cooling rate during solidification in the twin roll caster process, as well as the fact that the degree of supersaturation of the alloying elements, mainly Mn, is quite high [5] (the amount of solute in the solid solution was evaluated from electric conductivity measurements, as described below). Therefore, these three mechanisms can be acting at the same time. Accordingly, the twin roll caster sample has higher microhardness value when compared with the hot-rolled sample.

Conductivity versus solid−solution concentration

The relation between the electric conductivity, σ, and concentration of alloying elements in the solid solution of 3003 alloy can be expressed as follows [19]:

$$1/\sigma = 0.0267 + 0.032\mathrm{Fe_{ss}}\% + 0.033\mathrm{Mn_{ss}}\% + 0.0068\mathrm{Si_{ss}}\% + 0.0032\mathrm{Cu_{ss}}\%, \quad (1)$$

where $\mathrm{Fe_{ss}}\%$, $\mathrm{Mn_{ss}}\%$, $\mathrm{Si_{ss}}\%$, and $\mathrm{Cu_{ss}}\%$ are the weight percentages of the elements in solid solution.

Owing to the existence of this relation, supersaturation of alloying elements from the twin roll caster in relation to hot-rolled processes can be explained by comparing the electric conductivity of material produced by the two processes. Equation 1 shows that $\mathrm{Si_{ss}}\%$ and $\mathrm{Cu_{ss}}\%$ have a smaller influence on the electric conductivity than $\mathrm{Mn_{ss}}\%$. Besides, measurements on as-cast 3003 alloy ingots have shown that most of the Fe forms intermetallic particles, while a large amount of Mn is in solid solution during solidification [19]. On the other hand, variations in conductivity originating from crystalline defects are disregarded. Therefore, electric conductivity measurement may

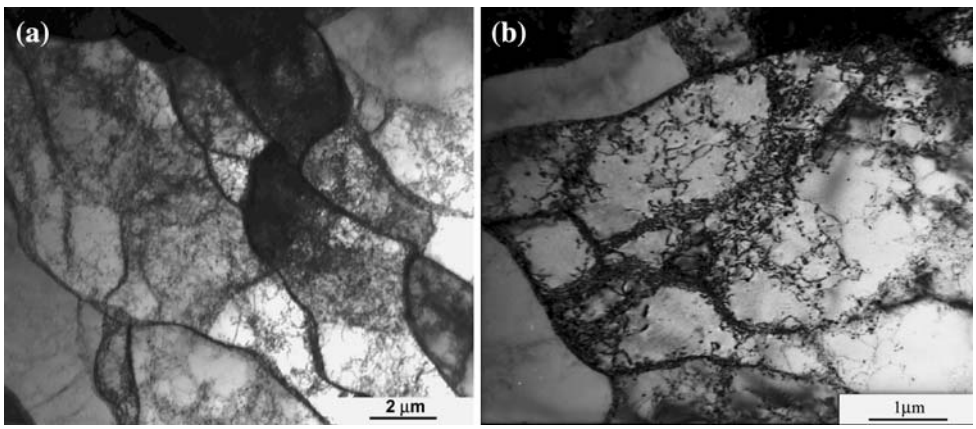

Fig. 1 Microstructure of the twin roll caster sample revealing the presence of both subgrains and dislocations into subgrains by transmission electronic microscopy (TEM). Samples were polished by electrolytic solution containing $HClO_4$

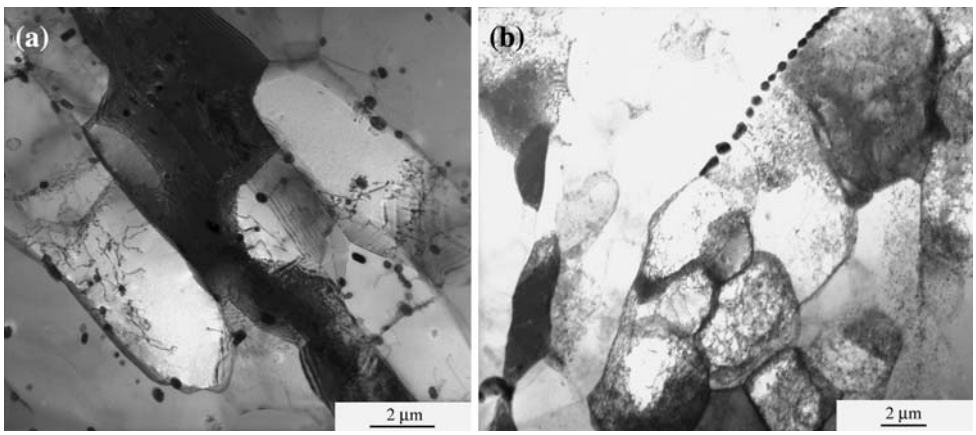

Fig. 2 Microstructure of the hot-rolled sample showing presence of subgrains structure and dislocations cellular structure in the interior subgrain, as well as presence of dispersoid by transmission electronic microscopy (TEM). Samples were polished by electrolytic solution containing $HClO_4$

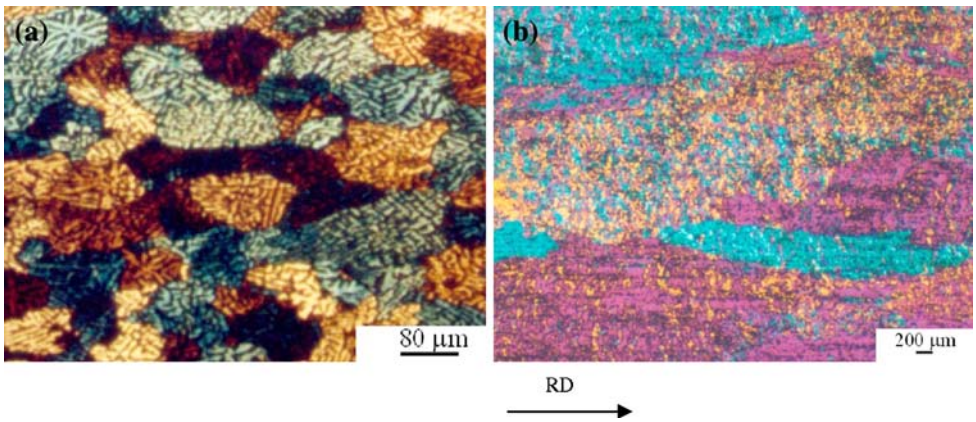

Fig. 3 **a** Surface microstructure of the twin roll caster sample illustrating dendrite structure in the interior grains and **b** surface micrography of the hot-rolled sample, with no dendrite structure observed (both by light microscopy with polarized light). Samples were anodized with solution containing HBF_4 (fluoboric acid)

be performed to estimate the Mn concentration in solid solution and gives a detailed indication of the decomposition reaction of the supersaturated solid solution during thermomechanical processing. The experimental results show that the electric conductivity measured from the twin roll caster sample is 29.9%, while that from the hot-rolled sample was 40.8%, that is, in the twin roll caster sample has appreciable supersaturation of alloying elements in solid solution when compared with the hot-rolled sample. When thermal treatment homogenization for 12 h at 500 °C is performed in the twin roll caster sample, the conductivity value increases from 29.9% to 49%, indicating decreasing solute in solid solution from precipitation.

Microstructural characterization

Figure 1 shows TEM micrographs revealing subgrain structure and presence of cellular structures within subgrains. Namely, dislocations are formed during twin roll caster processing and rearrange into subgrains and cellular structures. Cellular structures dislocations are evidence of the occurrence of plastic deformation at high temperature during twin roll caster processing [20]. It is also possible to observe the presence of elongated precipitates on subboundaries.

Subgrains formation is a recovery process [21]. For occurrence of cross slip and climb on a large scale is required higher thermal activation [22]. Therefore, the subgrains are formed at high temperature. However, the dislocations inside subgrains are formed at lower temperatures. The cooling speed in the twin roll caster process is quite high (200–700 °C/s). This suggests that formation of subgrains may be occurring at the beginning of the process, while dislocations in the interior subgrains appear at the end of the process.

It is also possible to observer in Fig. 2 the presence of subgrains in the hot-rolled sample. In this case, dislocations are formed during hot deformation and rearrange themselves in subgrains. The existence of small particles of 0.2 μm is also noticed, both in grains and on subboundaries, as well as dislocations around dispersoid.

Figure 3a, b show microstructures by light microscopy with polarized light from the twin roll caster and hot-rolled processes, both on surface regions. It is possible to observe in Fig. 3a dendrite structure in the interior grains from the twin roll caster process, while for the hot-rolled samples such structure is not observed (Fig. 3b). On the other hand, Fig. 3b shows larger grain size when compared with the twin roll caster sample (Fig. 3a). This reveals that grains are deformed because of rotation that they suffer relative to their neighborhood during plastic strain, thus resulting in heterogeneous coloration regions, as illustrated in Fig. 3b.

Figure 4a, b illustrate the microstructural features from the twin roll caster sample in the transversal and longitudinal directions, respectively. They reveal that the fine grain size distribution is homogeneous through the thickness. In the central region and at one-quarter thickness, grains are relatively equiaxial, suggesting that deformation during casting was accentuated at the surface. However, the microstructures of the hot-rolled samples change quite a lot through their thickness.

Table 3 presents the precipitate volumetric fraction measurement by light-microscopy dark-field technique followed by image analysis carried out in the three regions from the twin roll caster and hot-rolled samples. It can be clearly seen from Table 3 that the twin roll caster strip has higher precipitate volumetric fraction through its thickness in comparison with the hot-rolled strip, while on the surface both have equivalent values. This tendency is indicated in Fig. 5a–c, from which it can be inferred that precipitation occurs most often in the central region (Fig. 5a).

It is interesting to notice that, although there is difference of precipitate volumetric fraction through the thickness, the same does not occur in the chemical composition after the twin roll caster process, as shown by Table 1.

In addition, investigation in relation to fluid flow and heat transfer based on mathematical models [23] reveals

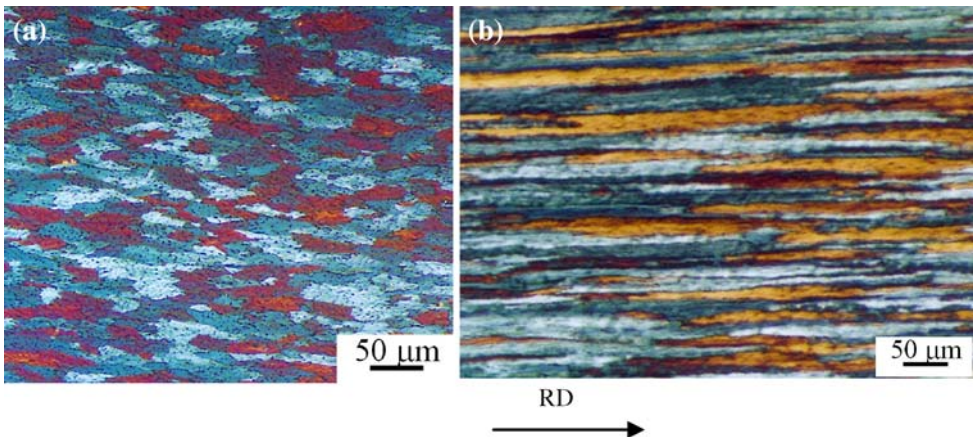

Fig. 4 **a** Microstructure of twin roll caster sample (transversal section) and **b** microstructure of caster sample (longitudinal section), both by light microscopy with polarized light. The images reveal that the fine grain size distribution is homogeneous through the thickness. Samples were anodized with solution containing HBF_4 (fluoboric acid)

Table 3 Precipitate volumetric fraction measurements through the thickness of strip from the twin roll caster and hot-rolling processes

Position	Twin roll caster	Hot rolling
Surface	4.2 ± 0.8	4.02 ± 1.1%
Quarter thickness	5.2 ± 0.7	3.60 ± 0.8%
Half thickness	6.3 ± 0.9	4.08 ± 0.7%

that there are levels or temperature boundaries, that is, while the temperature on the surface strip is lower (for instance, 300 K for Al–4.5%Cu alloy) due to contact with the water-cooled rollers, the temperature in the liquid zone region (as described in the "Microstructure" section) is quite high (i.e., 920 K for Al–4.5%Cu alloy). This temperature difference through the thickness can explain the higher precipitate volumetric fraction in the central region (at half thickness) for the twin roll caster sample. Consequently, the sustained higher temperature makes diffusion of alloying elements easier at the center of the strip, contributing to the occurrence of greater precipitation during cooling, as presented in Table 3.

Furthermore, with help of light microscopy the average precipitate size from the twin roll caster samples was also determined, as shown in Fig. 6. In this case, particles smaller than 0.5 μm were not considered, as they would be below the resolution limit of the light microscopy.

The twin roll caster process displayed considerable variation in the distribution of second-phase particles through the thickness. This can be seen in Fig. 7, which shows micrographs next to the surface (Fig. 7a) and in

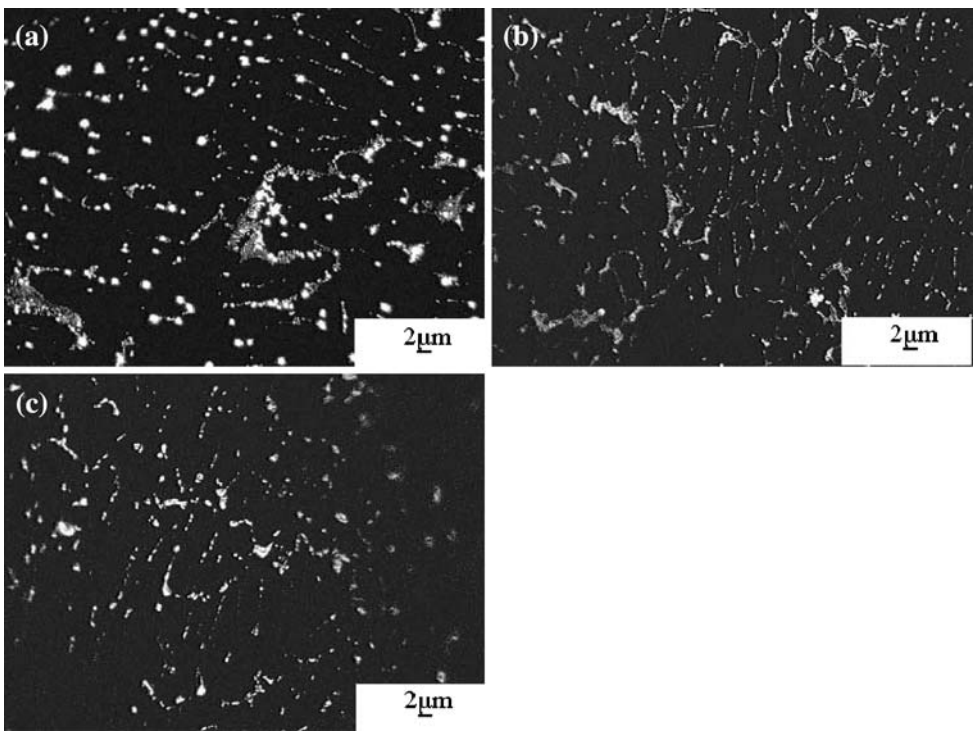

Fig. 5 Examples of images obtained by dark-field light microscopy for the determination of precipitates volumetric fraction: **a** twin roll caster, half thickness; **b** twin roll caster, quarter thickness; **c** twin roll caster, surface. Magnification 1,000×

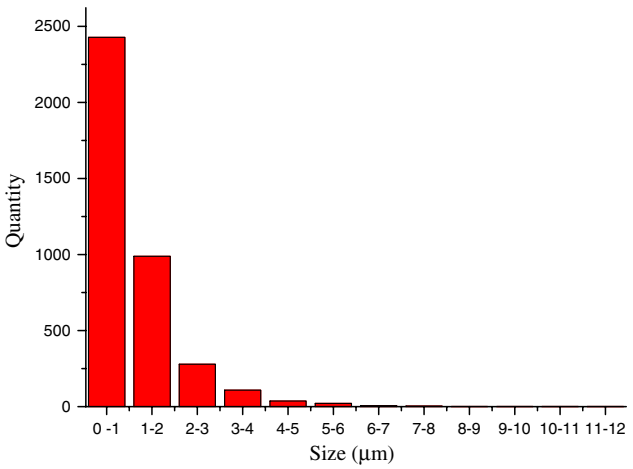

Fig. 6 Distribution of average precipitates size (by light microscopy) for the twin roll caster sample. In this case, particles smaller than 0.5 μm were not considered, as they would be below the resolution limit of the light microscopy

central regions (Fig. 7b), both obtained by SEM in backscattered mode. Thus, while the region next to the surface presents individualized particles and in lower amount, the central region shows considerable incidence of lamella colonies situated at interdendritic regions. It is interesting to remember that the lightest regions in Fig. 7, in backscattered mode, such as precipitates, indicate very high average atomic number, in other words, are richer in Mn and Fe than the matrix. This type of behavior is expected as elements that form eutectics such as Fe, Mn, and Si in general segregate at interdendritic regions. Microstructure of as-cast aluminum alloys in general presents dendritics with central enrichment in aluminum and in elements forming peritectics ($k > 1$), while elements forming eutectics ($k < 1$) concentrate at interdendritic regions. The distribution coefficient (k) is the quotient between the solid solute (C_S) and liquid solute (C_L) concentrations. Elements forming peritectics act additionally as refiners of grains.

Moreover, primary particles $Al_6(Mn,Fe)$ [24] were found very often in the twin roll caster strip, as can be seen in Fig. 8a, b. From electron diffraction images (Fig. 9) the precipitate Al_6Mn is observed.

From the precipitates, extraction technique was possible to detect presence of Al_6Mn and α-AlMnSi phases from the twin roll caster samples, as shown in Fig. 10. The peaks of higher intensity of Al_6Mn and α-AlMnSi phases are between intervals of (2θ value) 36° and 46° (Fig. 10). In the present case, the difficulty is related to the fact that both interplanar distance and 2θ values are equivalent for the two phases. Therefore, the slowest scan was performed (exposure time of 10 s) to decrease noise, in order to differentiate peaks from the noise. The peaks of Al_6Mn and α-AlMnSi phases were identified with the support of JCPDS 06-0665 and 06-0669 index cards, respectively. As a result, from both interplaner distance and corresponding reflection (2θ) values, the lattice parameters were calculated. For the cubic phase, the Cohen method was applied [25], thus obtaining the value of 1.262 nm. For the orthorhombic phase, the following parameters value were found: $a = 0.651$ nm, $b = 0.737$ nm, and $c = 0.881$ nm, in accordance with the investigation of Cook et al. [10]. During the performance of precipitates extraction it was not possible to dissolve all the aluminum matrix, but it was possible to index the corresponding peaks of the phases present. It can be seen from Fig. 10 that the amount of Al_6Mn phase is higher than that of α-AlMnSi phase.

Texture evaluation

Texture evaluation of the strips was performed through their thickness (on the surface, one-quarter thickness, and

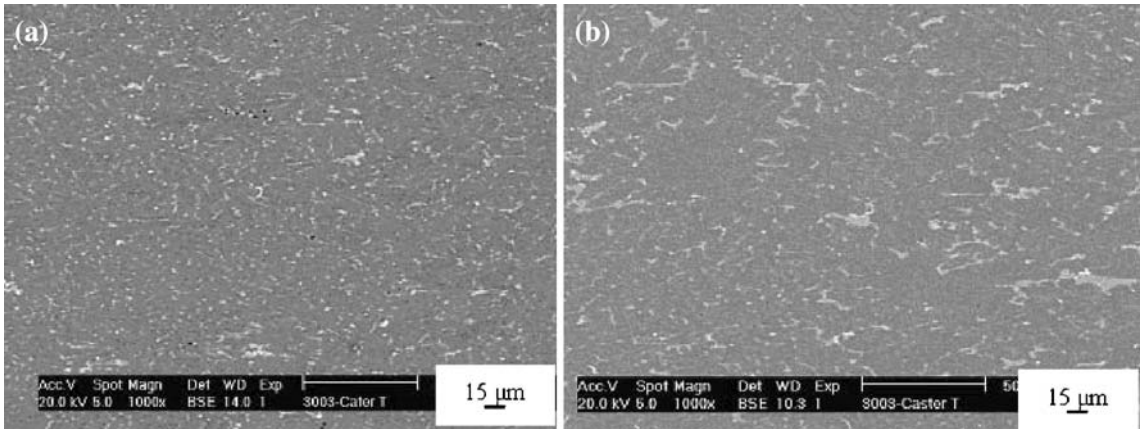

Fig. 7 Images obtained by backscattered electron SEM of the twin roll caster strip: **a** region next to the surface, showing individualized particles and in lower amount, and **b** central region, showing considerable incidence of lamella colonies situated at the interdendritic regions. Samples were etched with solution containing HBF_4 (fluoboric acid)

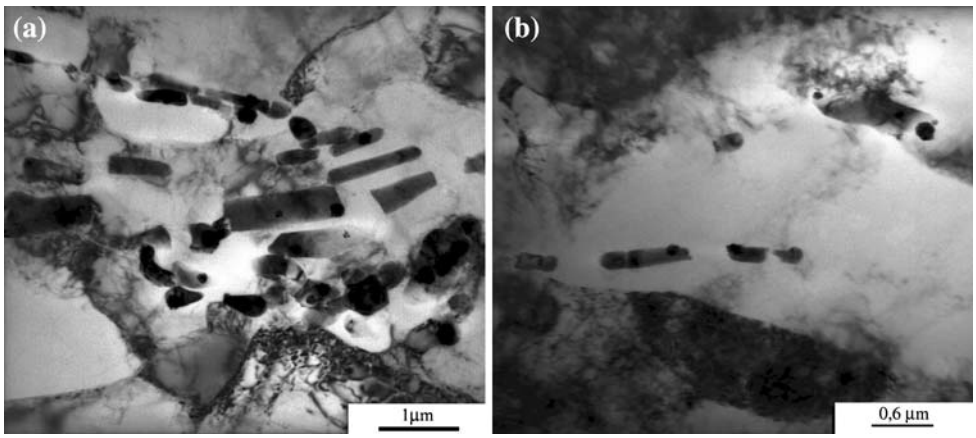

Fig. 8 **a** Microstructure of the twin roll caster sample showing the presence of several rectangular precipitates (Al_6Mn) and **b** microstructure of the twin roll caster sample, exhibiting presence of dispersoids, both by TEM. Samples prepared with electrolytic solution containing $HClO_4$

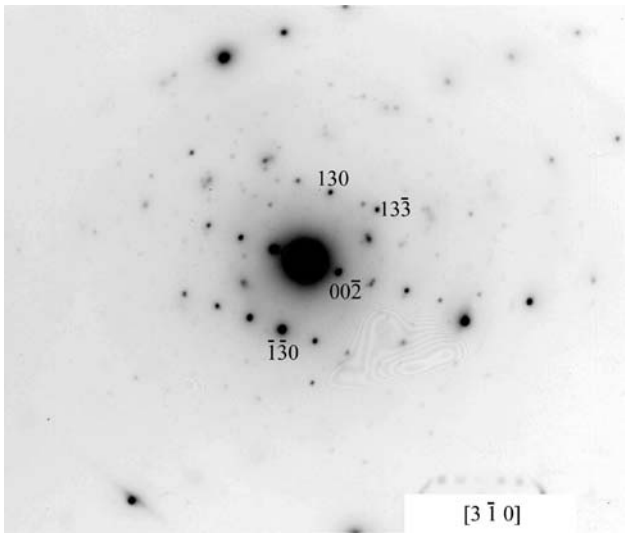

Fig. 9 Precipitate Al_6Mn by electron diffraction found in the twin roll caster sample. The direction of the electron beam is indicated in the micrograph

in the center) by X-ray diffraction technique for both the twin roll caster and hot-rolled samples. A more complete description concerning texture can be obtained with the help of the ODF of grains. These functions specify the frequency of occurrence of determined orientations in a three-dimensional space, defined by three Euler angles: φ_1, ϕ, and φ_2. The ODF is calculated through by the PF obtained by X-ray diffraction. Figure 11 shows the location in Euler space of the most important texture components in FCC metals rolling [26]. These components involve the α-fiber between Goss $\{011\}\langle 100\rangle$ and brass $\{110\}\langle 1\bar{1}2\rangle$ and β-fiber between brass and copper $\{112\}\langle 11\bar{1}\rangle$, and component of type S $\{123\}\langle 63\bar{4}\rangle$.

On the surface region of the twin roll caster sample the presence of component $\{001\}\langle 110\rangle$ ($\varphi_1 = 45°$, $\phi = 0°$ or 90°, $\varphi_2 = 0°$) was observed (Fig. 12), well known as a rotated cube, with intensity 26.3. While, in the central region (Fig. 13) the presence of three components: (a) type brass ($\varphi_1 = 35°$, $\phi = 45°$, $\varphi_2 = 0°$) higher intensity $f(g) = 13.6$, (b) type S ($\varphi_1 = 59°$, $\phi = 34°$, $\varphi_2 = 65°$) with $f(g) = 11.7$, and (c) type copper ($\varphi_1 = 90°$, $\phi = 30°$, $\varphi_2 = 45°$) with $f(g) = 9.7$ was verified. At quarter thickness, the presence of component of type brass, with $f(g) = 10.3$, can be noted. On the other hand, the Goss component ($\varphi_1 = 0°$, $\phi = 45°$, $\varphi_2 = 0°$) appears in the ODF in Fig. 14; it is related to the ghost phenomenon, because the PF were analyzed and this component was not found. However, studies performed by Singh and Singh [27] showed that there is increase in intensity of the Goss component through the thickness, which can be attributed to lower cooling rates during and after hot rolling.

On the other hand, the texture of the hot-rolled strip was also analyzed through its thickness, i.e., in the three regions, as illustrated in Figs. 15, 16, and 17, respectively. From Fig. 15 (on the surface) the ODF reveals the presence of $\{001\}\langle 110\rangle$ component, known as a rotated cube. It appears with intensity of 28. Daaland and Nes [28] also found strong presence of $\{001\}\langle 110\rangle$ component below the surface (until one-third thickness) from hot-rolled strip of Al1Mn0.5Mg alloy. However, in Fig. 16 (at quarter thickness) the ODF from the hot-rolled sample shows the presence of $\{011\}\langle 21\bar{1}\rangle$ component, type brass, of intensity 15.6. From Fig. 17 (in the center), the ODF has the same features as observed in Fig. 15.

Lee et al. [29] have proposed that subdivision of orientations into polycrystalline grains promotes the formation of brass-type component that frequently occurs during hot rolling.

Mesotexture analysis was also performed to characterize the nature of the boundaries of the twin roll caster and hot-rolled samples, as shown in Fig. 18a, b, respectively. It is possible to observe for both conditions that light boundaries indicate high-angle boundaries ($\psi > 15°$) while the black boundaries are low angle ($\psi < 15°$), as can be inferred from Fig. 18a, b. This also shows that in the strongly textured region there is a high fraction of

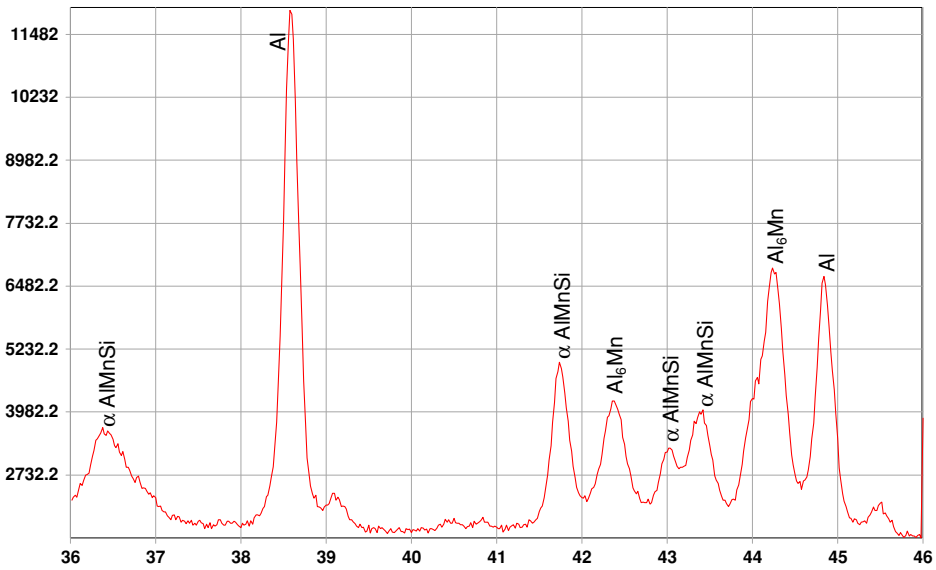

Fig. 10 X-ray diffraction (using copper pipe) from the twin roll caster sample residue by electrolytic dissolution with solution containing $HClO_4$. Slow scanning was performed, with exposure time of 10 s

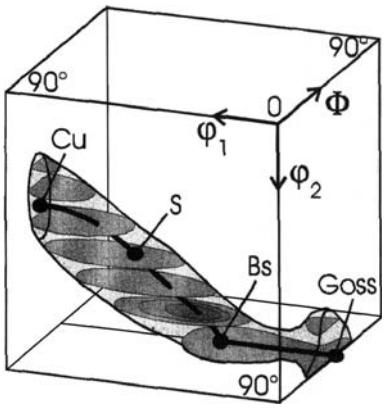

Fig. 11 Texture components of the CBC metals rolling in 3D Euler space: β-fiber between copper and brass components, and α-fiber between the component of type brass and Goss [26]

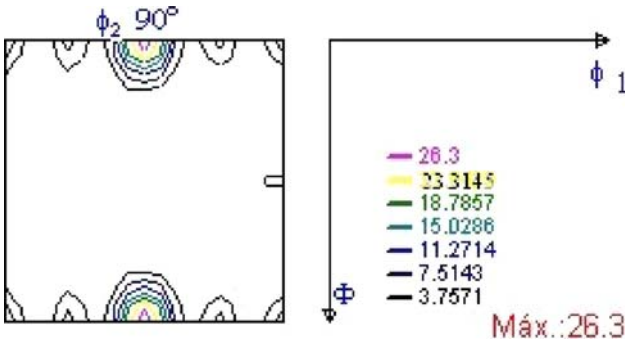

Fig. 12 ODF (X-ray diffraction) on the surface of the twin roll caster sample, showing the presence of component $\{001\}\langle 110\rangle$ ($\varphi_1 = 45°$, $\phi = 0°$ or 90°, $\varphi_2 = 0°$), well known as a rotated cube, with intensity 26.3

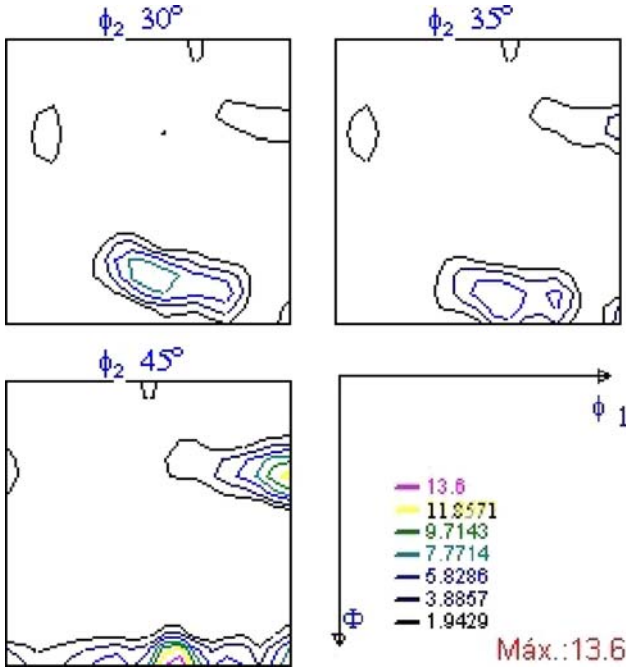

Fig. 13 ODF (X-ray diffraction) in the region (quarter thickness) of the twin roll caster sample, showing the presence of three components: type brass ($\varphi_1 = 35°$, $\phi = 45°$, $\varphi_2 = 0°$) higher intensity $f(g) = 13.6$, type S ($\varphi_1 = 59°$, $\phi = 34°$, $\varphi_2 = 65°$) with $f(g) = 11.7$, and type copper ($\varphi_1 = 90°$, $\phi = 30°$, $\varphi_2 = 45°$) with $f(g) = 9.7$

low-angle boundaries for the two conditions. This characteristic of small difference of orientations (1–5°) has been found in as-cast aluminum alloy [30]. These small differences of orientation in the interior of grains appear during dendritic solidification, between different dendritic arms growing from a core owing to dendritic structure bending in the two phases, i.e., solid–liquid state. However, the high fraction of low-angle boundaries for hot-rolled samples is attributed to deformation during process.

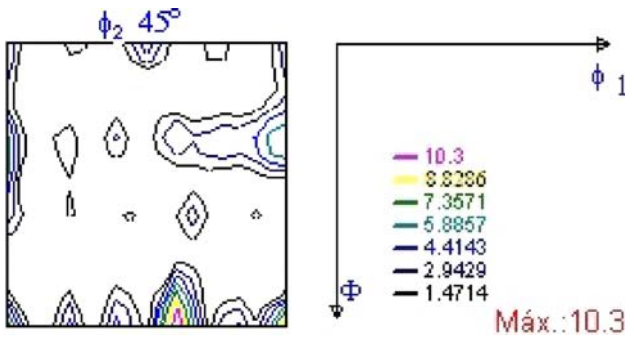

Fig. 14 ODF (X-ray diffraction) in the region (quarter thickness) of the twin roll caster sample, showing the Goss component ($\varphi_1 = 0°$, $\phi = 45°$, $\varphi_2 = 0°$). In this case it is related to the ghost phenomenon

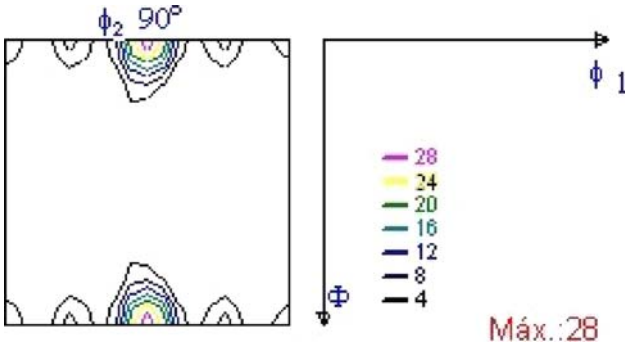

Fig. 15 ODF (X-ray diffraction) on the surface of the hot-rolled sample, revealing presence of $\{001\}\langle 110\rangle$ component, known as a rotated cube, which appears with intensity of 28

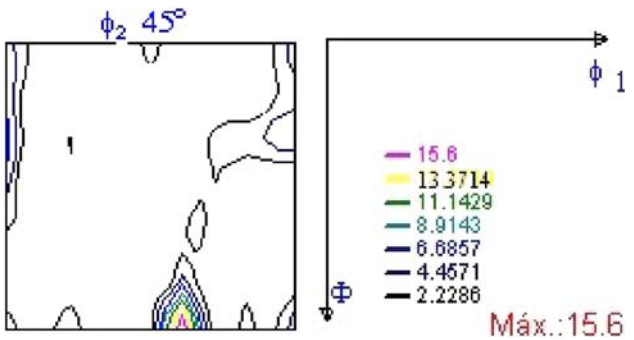

Fig. 16 ODF (X-ray diffraction) in the region of quarter thickness of the hot-rolled sample, showing presence of $\{011\}\langle 21\bar{1}\rangle$ component, type brass, of intensity 15.6

Concluding remarks

The present study has investigated and compared microstructure and texture evolution of two strips of Al–Mn–Fe–Si (3003) aluminum alloy produced by continuous casting (twin roll caster) and semicontinuous casting (direct chill

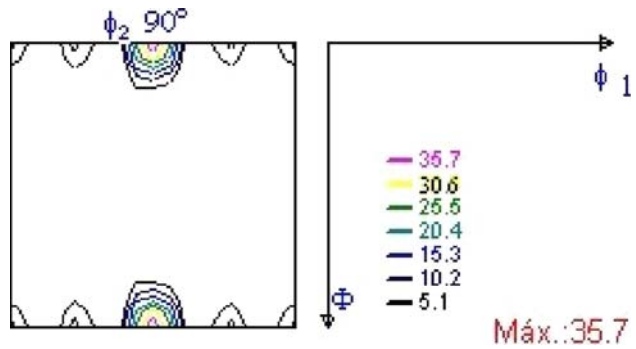

Fig. 17 ODF (X-ray diffraction) in the region of half thickness of the hot-rolled sample, revealing presence of $\{001\}\langle 110\rangle$ component, known as a rotated cube, which appears with intensity of 28

followed by hot rolling) processes. The results obtained can be summarized as follows:

- During twin roll caster processing there is considerable plastic deformation and corresponding formation of subgrains and dislocation cells.
- The difference in microhardness between both twin roll caster and hot-rolled strips is attributed to three mechanisms: (a) deformation hardening, (b) refine-grain hardening, and (c) incoherent precipitates dispersion hardening.
- Microstructure and grain morphology (in longitudinal and transversal directions) for the twin roll caster strip are more homogeneous compared with for the hot-rolled strip, and the grain size for the hot-rolled strip is much higher.
- In the twin roll caster strip there is supersaturation of alloying elements, especially Mn in solid solution, when compared with the hot-rolled strip.
- In both processes, the chemical composition does not change through the thickness of the strip. For the twin roll caster strip the precipitates volumetric fraction is higher in the central region, which is associated with two factors: the temperature gradient through its thickness and the cooling rate.
- The strips from both processes display strong texture gradient through their thickness. Type $\{011\}\langle 211\rangle$ brass is predominant. Another important component is the rotated cube $\{001\}\langle 110\rangle$, which predominates on the surface. However, the main difference in texture through the thickness between the two processes was found in the central region (halfway thickness). In the twin roll caster strip three types were found: S, copper, and brass components. In the other strip only the rotated cube component appears.
- Texture on the surface of the twin roll caster strip is typical of hot rolling.

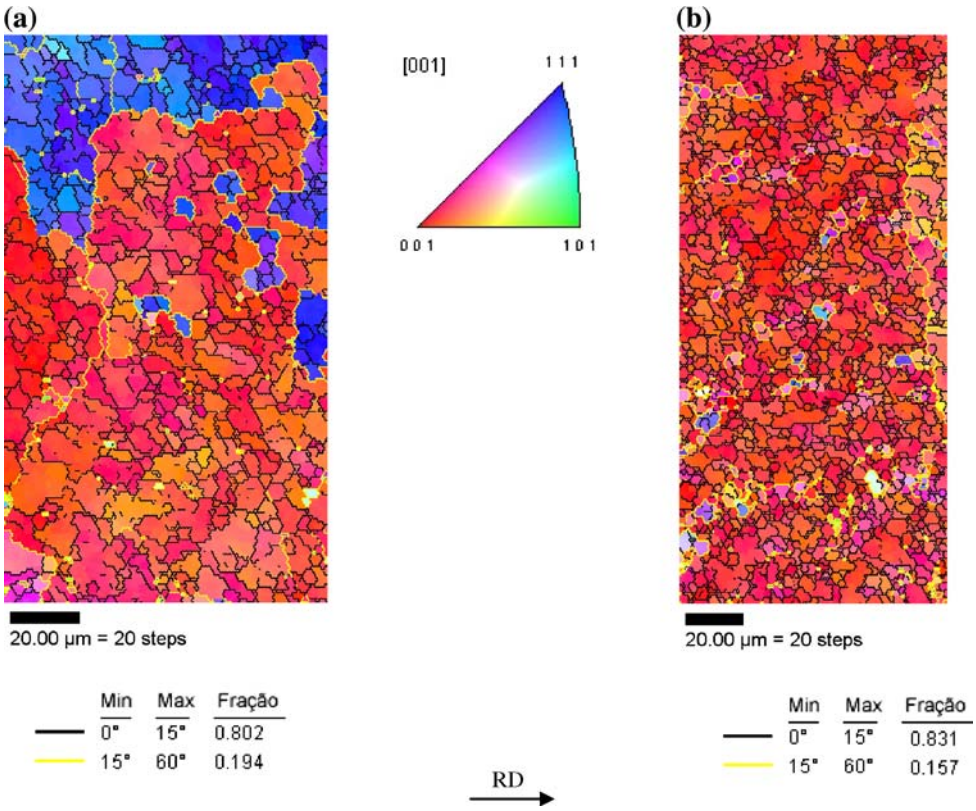

Fig. 18 **a** Orientation image mapping from ESBD data on the surface of the twin roll caster. **b** Orientation image mapping from ESBD data on the surface of the hot-rolled sample

Acknowledgements This work is supported by the Fundação de Amparo à Pesquisa do Estado de São Paulo (FAPESP) through Grant 02/03252-6. Authors also acknowledge the technician Eliseu Evangelista de Oliveira (EPUSP-PMT-Grant 02/09910-5) for fundamental help during preparation of samples.

References

1. Mondolfo LF (1977) In: Bros P, Lane MC (eds) Manganese in aluminum alloys. The Manganese Centre, Nevilly sur Seine, p 118
2. Hatch JE (1990) Aluminum, properties and physical metallurgy. ASM, Metals Park, Ohio
3. Polmear J (1989) Light alloys—metallurgy of the light metals, 2nd edn. Edward Arnold, New York, p 278
4. Alexander DTL, Greer AL (2002) Acta Mater 50:2571
5. Berg BS, Hansen V, Zagierski PT, Nedreberg ML, Olsen A, Gjonnes J (1995) J Mater Process Technol 53:65
6. Strid J (1992) In: Proceedings from the 3rd international conference on Al alloys, vol 3. Trondheim, p 321
7. Merchant HD, Kattamis TZ, Morris JG (1989) In: Continuous casting of non ferrous metals and alloys. TMS, Warrendale, PA, p 1
8. Santos CA, Spim JA Jr, Garcia A (2000) J Mater Process Technol 102:33
9. Li BQ (1995) J Min Met Mater Soc (JOM) 47:29
10. Cook R, Grocock PG, Thomas PM, Edmonds DV, Hunt JD (1995) J Mater Process Technol 55:76
11. Lockyer SA, Ming Y, Hunt JD, Edmonds DV (1996) Mater Charact 37:301
12. Haga T (2001) J Mater Process Technol 111:64
13. Haga T, Suzuki S (2001) J Mater Process Technol 113:291
14. Hansen V, Andersso B, Tibballs JE, Gjonnes J (1995) Metall Mater Trans B 26:839
15. Slamova M, Karlik M, Robaut F, Slama P, Veron M (2003) Mater Character 49:231
16. Digital library of the thesis and master degree (2005) Brazil, Universidade de São Palulo. Retrieved September 15, 2008, from http://www.teses.usp.br/teses/disponiveis/3/3133/tde-31012006-124433/
17. Tricibar R, Jin I (1999) In: Light metals. TMS publications, Warrandale, PA, p 1129
18. Westengen H (2000) In: Light metals. TMS publications, Warrandale, PA, p 1111
19. Li YJ, Arnberg L (2003) Acta Mater 52:3415
20. Humphreys FJ, Hatherly M (1995) Recrystallization and related annealing phenomena. Oxford, Pergamon, p 497
21. Blum W, Schlögl C, Meier M (1995) Zeitschrift für Metallkunde 86:631
22. Martin JW, Doherty RD, Cantor B (1997) Stability of microstructure in metallic systems, 2nd edn. Cambridge University Press, Cambridge, p 426
23. Saxena A, Sahai Y (2002) Mater Trans 43:206
24. Sperry PR (1955) J Metals 7:145
25. Cullity BD, Stock SR (2001) In: Elements of X-ray diffraction, 3rd edn. Prentice Hall, New Jersey, p 664
26. Maurice CI, Driver JH (1997) Acta Mater 45:4627
27. Singh RK, Singh AK (1998) Scripta Mater 38:1299
28. Daaland O, Nes E (1996) Acta Mater 44:1413
29. Lee CS, Duggan BJ, Smallman RE (1993) Acta Metall Mater 41:2265
30. Samajdar I, Doherty RD (1994) Scr Metall Mater 31:527